**SUPPLEMENTARY MATERIAL**

## Supplementary Methods

### *Immunotherapy-treated lung cancer patients*

Patients in the training cohort (MCC1) were enrolled in industry-sponsored clinical trials between June 2011 and January 2016 at Moffitt Cancer Center. Majority of the patients (94.6%) in MCC2 cohort treated with standard-of-care immunotherapy between May 2015 and October 2017 at Moffitt Cancer Center. Patients in the VA cohort were treated with standard-of-care immunotherapy between July 2015 and February 2019 at the James A. Haley Veterans' Hospital. Patient data were obtained using electronic medical records and institutional databases.

Common inclusion criteria for clinical trial patients included: patients who were diagnosed with histologically- or cytological-documented NSCLC with advanced/metastatic stage disease with at least one measurable lesion (≥ 10 mm), Eastern Cooperative Oncology Group (ECOG) Performance Status of 0 or 1, and provided written informed consent. Common exclusion criteria included: a concurrent medical condition requiring the use of immunosuppressive medications or immunosuppressive doses of systemic or absorbable topical corticosteroids, and presence of any active autoimmune disease.

Moffitt's Cancer Registry abstracts information from patient electronic medical records on demographics, history of smoking, stage, histology, RECIST, treatment, and vital status. Follow-up for vital status occurs annually through active (i.e., chart review and directly contacting the patient, relatives, and other medical providers) and passive methods (i.e., mortality records). Hematology data were obtained from the CDCS and included: lactate dehydrogenase (LDH), serum albumin, lymphocytes, white blood cells (WBC), neutrophils, fibrinogen, and neutrophil to lymphocyte ratio (NLR). Manually abstracted data included: targeted mutations (*EGFR, KRAS*), history of systemic treatment(s) for current lung cancer staging, ECOG

performance status, number of metastatic sites (number of organs that have metastatic lesions), and metastatic sites prior to treatment. Date of progression was abstracted and defined as progressive disease from RECIST or iRECIST definition or clinical progression evaluated by the treating clinicians whenever RECIST data was not available. There was loss to follow-up for 85 (47%), 42 (27%) and 27 (44%) patients in the training, validation 1, and validation 2 cohorts, respectively. The median follow-up time for the patients who were loss to follow-up was 20, 17, and 13 months for training, validation 1 and validation 2 cohorts, respectively. All patient data collected from James A. Haley Veterans' Hospital (VA cohort) were manually collected from electronic medical records of the patients.

***Radiomic feature extraction***

Peritumoral regions were bounded by the lung parenchyma mask to exclude any peritumoral delineation that exceeds outside of the lung parenchyma. Unstable and non-reproducible radiomic features were eliminated using methods described elsewhere [1] utilizing two publicly available datasets [2, 3]. The "Moist-run" dataset [2] was utilized to identify stable features which consist of 40 CT images of lung tumors with three different segmentation algorithms and three different initialization parameters (e.g., seed point) for each segmentation. The Reference Image Database to Evaluate Therapy Response (i.e., RIDER) test-retest dataset [3] was used to identify reproducible features which consists of 32 lung cancer patients who had two non-contrast chest CT scans acquired 15 minutes apart using the same scanner, acquisition, and processing parameters. Stable features were identified by assessing the concordance correlation coefficient (CCC) between radiomic features extracted using different segmentations from the "Moist-run" dataset. Reproducible features were identified by assessing the CCC between radiomic features extracted test and the retest scans from the RIDER dataset.

The CT images were resampled to a single voxel spacing of 1mm x 1mm x 1mm using cubic interpolation to standardize spacing across all images. Hounsfield units (HU) in all CT images were then resampled into fixed bin sizes of 25 HUs discretized from –1000 to 1000 HU.

***Definitions of the Radiomic features***

*Grey level co-occurrence matrix-based features*

The grey level co-occurrence matrix (GLCM) has been proved to be a powerful approach for image texture analysis. The GLCM is a matrix that expresses how combinations of discretized grey levels of neighboring pixels (or voxels in 3-dimensional space) in a region-of-interest are distributed along one of the spatial image directions. In other words, it describes how often a pixel of grey level *i* appears in a specific spatial relationship to a pixel of grey level *j*. Hence GLCM matrix defined as P where each matrix element $\mathrm{p_{ij}} = \mathrm{P(i,j)}$ represents the number of times a grey level i is neighbors with voxels of grey level j with an inter-pixel distance and orientation. The GLCM defines a square matrix whose size is equal to the largest grey level $\mathrm{N_g}$ appearing in the region-of-interest. Haralick et al (Haralick et al. IEEE Trans Syst Man Cybern, 6:610-621,1973) proposed 14 original statistics (e.g., contrast, correlation, energy) to be applied to the GLCM to measure the texture features. The GLCM inverse difference feature (i.e., “avatar” feature) is a measure of homogeneity, where the feature quantity is greatest if all grey levels are the same. Inverse difference is defined as follows:

$$F_{glcm.inv.diff} = \sum_{i=1}^{N_g}\sum_{j=1}^{N_g}\frac{p_{ij}}{1+|i-j|}$$

where $\mathrm{N_g}$ is the number of discretized grey levels inside the region-of-interest.

The seven features that were found to be correlated with GLCM inverse difference were presented in Figure 2B. The definitions for these seven features are presented below.

i) *GLCM inverse variance*:

$$GLCM_{inverse\ variance} = 2\sum_{i=1}^{N_g}\sum_{j>1}^{N_g}\frac{p_{ij}}{(i-j)^2}$$

*Grey level run length-based features*

The grey level run length matrix (GLRLM) features were first presented by Galloway (M. Galloway, Computer Graphics and Image Processing, 4:172-179, 1975) to quantify texture of an image or region-of-interest. GLRLM is a matrix that consists of counts of the grey level run lengths along a desired spatial direction. A GLRLM is defined as R where each matrix element $\mathrm{R(i,j)}$ represents the number of runs of a grey level i of length j. Hence the GLRLM is sized $\mathrm{N_g\ x\ N_r}$. Four features utilizing GLRLM were found to be correlated with GLCM inverse difference (Figure 2B).

i) *Avg 3D RLV (Run length variance)*:

$$GLRLM_{rlv} = \sum_{i=1}^{N_g}\sum_{j=1}^{N_r}(j-\mu)^2 p_{ij}$$

$$\text{Where } \mathrm{p_{ij} = r_{ij}/N_s} \text{ and the mean run length } \mu = \sum_{i=1}^{N_g}\sum_{j=1}^{N_r} j\, p_{ij}$$

ii) *Avg 3D LRE (Long runs emphasis)*:

$$GLRLM_{lre} = \frac{1}{N_s}\sum_{j=1}^{N_r} j^2 r_j$$

where $r_j = \sum_{i=1}^{N_g} r_{ij}$.

iii) *Avg 3D RP (Run percentage)*:

$$GLRLM_{rp} = \frac{N_s}{N_v}$$

Where $N_v$ is the total number of voxels in a region-of-interest (ROI).

iv) *Avg 3D SRE (Short runs emphasis)*:

$$GLRLM_{sre} = \frac{1}{N_s}\sum_{j=1}^{N_r} \frac{r_j}{j^2}$$

v) Avg 3D RLN normalized (Run length non uniformity normalized):

$$GLRLM_{rln} = \frac{1}{N_s^2}\sum_{i=1}^{N_g} r_i^2$$

*Grey level size zone-based features*

The grey level size zone matrix (GLSZM) counts the number of groups (i.e., zones) of connected pixels with an explicit discretized grey level value and size and was first proposed by Thibault et al (Thibault et al. 2014). The voxel connectedness depends on the desired definition of connectedness where in 3 dimensional approaches is 26-connectedness and in 2 dimensional approaches is 8-connectedness. A

GLSZM defined as S is sized as $N_g$ x $N_z$ where $N_g$ is the number of discretized grey levels in the region-of-interest and $N_z$ is the maximum zone size. Each element $s_{ij} = s(i, j)$ is the number of zones with discretized grey level i and size j.

One feature utilizing GLSZM were found to be correlated with GLCM inverse difference (Figure 2B).

i) *GLSZM low grey level zone emphasis*:

$$GLSZM_{glze} = \frac{1}{N_s} \sum_{i=1}^{N_g} \frac{s_i}{i^2}$$

where $s_j = \sum_{i=1}^{N_g} s_{ij}$.

***Stable and reproducible features***

Two separate publicly available datasets (downloaded from: http://www.cancerimagingarchive.net) were utilized to assess stability (The Moist-run dataset [2]), and reproducibility (RIDER dataset [3]) of radiomic features to increase the likelihood of a reproducible and robust radiomics model.

The Moist-run dataset was constructed by the Quantitative Imaging Network (QIN) as part of a lung segmentation challenge [2] and consists of 40 chest CT images of 40 NSCLC patients and one thoracic phantom from five collections of Digital Imaging and Communications Medicine series. Each patient in the dataset had one lesion of interest and the thoracic phantom scan had 12 lesions of interest. The RIDER test-retest dataset which was used to find the reproducible features [3] consisted of 32 NSCLC patients with two separate non-contrast CT scans acquired within 15 minutes of each other using the same scanner with fixed acquisition and

processing parameters. As such, the only variation between the test and retest scans were attributed to patient orientation, respiratory, and movement. The images on these datasets were previously de-identified

Using the Moist run dataset, all radiomic features were computed for 9 different segmentations done by 3 different algorithms which each were run by 3 different initial parameters. Afterwards, concordance correlation coefficient (CCC) metric was calculated to assess inter- and intra-segmentation differences of the radiomic features. The RIDER dataset was utilized to assess reproducibility of radiomic features between test and re-test scans. After extracting radiomic features from both scans of the patients, CCC values were calculated and features that have a CCC < 0.75 were eliminated. Shape features were only extracted from intratumoral regions as they were proven to be highly correlated (Pearson correlation > 0.95) with their peritumoral versions.

***Gene expression data for the radiogenomic analyses***

Gene expression was IRON-normalized and batch-corrected for RNA quality and Pathway and Gene Ontology Enrichment was performed using Clarivate Analytics MetaCore [4]. For the radiogenomics analysis, the most informative radiomic feature was compared to every gene probesets using two different approaches: correlation and two-group analysis. For the correlation analysis, gene probesets were filtered and determined as statistically significant using the following criteria: Pearson's correlation with a threshold $|R| > 0.4$, an expression filter with max expression of gene > 5, and an inter-quartile filter (interquartile range > log2 (1.2 fold-changes). Gene probesets were filtered and determined as significant using the following criteria based on a Student's t test $P < .001$ and mean log fold-changes (LFC) between high and low prognostic radiomic feature of LFC > log2 (1.4 fold-changes). The significant probesets from the two analyses were intersected yielding a final list of probesets significantly associated with the prognostic radiomic feature.

***IHC staining procedures for CAIX (human expression)***

Slides were stained using a Ventana Discovery XT automated system (Ventana Medical Systems, Tucson, AZ) as per manufacturer's protocol with proprietary reagents. Briefly, slides were deparaffinized on the automated system with EZ Prep solution (Ventana). Heat-induced antigen retrieval method was used in RiboCC (Ventana). The rabbit primary antibody that reacts to *CAIX*, (#ab15086, Abcam, Cambridge, MA) was used at a 1:250 concentration in Dako antibody diluent (Carpenteria, CA) and incubated for 32 min. The Ventana OmniMap Anti-Rabbit Secondary Antibody was used for 20 min. The detection system used was the Ventana ChromoMap kit and slides were then counterstained with Hematoxylin. Slides were then dehydrated, and cover slipped as per normal laboratory protocol.

***Positive pixel count algorithm***

Automated evaluation of positive staining percentage was defined by the Aperio ImageScope (http://www.leicabiosystems.com) Positive Pixel Count Algorithm which automatically calculates the ratio of the total number of positive stained pixels to the total number of tumor and its immediate microenvironment pixels.

## References

1. Tunali I, Hall LO, Napel S, et al. Stability and reproducibility of computed tomography radiomic features extracted from peritumoral regions of lung cancer lesions. Med Phys 2019; 10.1002/mp.13808.

2. Kalpathy-Cramer J, Zhao B, Goldgof D, et al. A Comparison of Lung Nodule Segmentation Algorithms: Methods and Results from a Multi-institutional Study. J Digit Imaging 2016;29(4):476-87.

3. Zhao B, James LP, Moskowitz CS, et al. Evaluating variability in tumor measurements from same-day repeat CT scans of patients with non-small cell lung cancer. Radiology 2009;252(1):263-72.

4. Schabath MB, Welsh EA, Fulp WJ, et al. Differential association of STK11 and TP53 with KRAS mutation-associated gene expression, proliferation and immune surveillance in lung adenocarcinoma. Oncogene 2016;35(24):3209-16.

## Supplementary Tables

Supplementary Table 1. Overall survival and progression free survival rates by patient risk groups for MCC1, MCC2, and VA cohorts[a]

| | Percent survival (95% CI) at: | | | |
|---|---|---|---|---|
| | 6 months (½ year) | 12 months (1 year) | 24 months (2 years) | 36 months (3 years) |
| Overall survival | | | | |
| *Overall* | | | | |
| MCC1 cohort | 82.7% (76.3-87.5) | 60.8% (52.8-67.9) | 42.1% (33.6-50.3) | 32.6% (23.8-41.6) |
| MCC2 cohort | 61.7% (50.7-70.9) | 46.2% (35.4-56.3) | 22.4% (13.5-32.8) | 19.2% (10.2-30.3) |
| VA cohort | 75.5% (62.7-84.5) | 63.0% (49.4-74.0) | 31.9% (17.9-46.9) | 12.0% (1.2-36.3) |
| *By risk group* | | | | |
| Low-risk | | | | |
| MCC1 cohort | 100% | 100% | 88.9% (62.4-97.1) | 88.9% (62.4-97.1) |
| MCC2 cohort | 95.0% (69.5-99.3) | 85.0% (60.4-94.9) | 38.9% (17.1-60.3) | 38.9% (17.1-60.3) |
| VA cohort | 91.7% (53.9-98.8) | 80.2% (40.3-94.8) | 80.2% (40.3-94.8) | 40.1% (1.3-83.5) |
| Moderate-risk | | | | |
| MCC1 cohort | 92.6% (81.5-97.2) | 76.4% (62.1-85.9) | 59.7% (44.0-72.4) | 47.9% (30.7-63.2) |
| MCC2 cohort | 67.8% (44.0-83.3) | 56.7% (32.7-75.0) | 33.1% (10.9-57.6) | n/a |
| VA cohort | 72.2% (45.6-87.4) | 66.2% (39.6-83.2) | 29.8% (9.7-53.4) | n/a |
| High-risk | | | | |
| MCC1 cohort | 81.4% (70.1-88.7) | 53.5% (40.0-65.2) | 24.5% (12.1-39.2) | 15.3% (5.0-30.9) |
| MCC2 cohort | 62.1% (42.1-76.0) | 34.1% (17.8-51.2) | 17.1% (5.4-34.4) | 8.5% (0.8-28.4) |
| VA cohort | 74.4% (48.9-88.5) | 57.2% (32.1-76.0) | 32.7% (7.4-61.8) | n/a |
| Very-high-risk | | | | |
| MCC1 cohort | 59.9% (41.8-73.9) | 24.3% (10.6-41.1) | 12.2% (3.2-27.6) | 0% |
| MCC2 cohort | 16.7% (4.1-36.5) | 11.1% (1.9-29.8) | 0% | 0% |
| VA cohort | 66.7% (33.7-86.0) | 47.6% (18.2-72.4) | n/a | n/a |
| Progression-free survival | | | | |
| *Overall* | | | | |
| MCC1 cohort | 47.9% (40.4-55.1) | 32.8% (25.7-40.0) | 22.8% (16.3-30.0) | 20.8% (13.9-28.5) |
| MCC2 cohort | 37.9% (27.7-48.0) | 19.6% (11.9-28.7) | 9.5% (4.0-18.0) | 9.5% (4.0-18.0) |
| *By risk group* | | | | |
| Low-risk | | | | |
| MCC1 cohort | 75.0% (50.0-88.8) | 75.0% (50.0-88.8) | 68.8% (42.9-84.7) | 68.8% (42.9-84.7) |
| MCC2 cohort | 73.7% (47.9-88.1) | 46.3% (23.2-66.7) | 29.8% (9.4-53.7) | 29.8% (9.4-53.7) |
| Moderate-risk | | | | |
| MCC1 cohort | 65.9% (51.4-77.0) | 43.0% (29.1-56.2) | 31.2% (18.6-44.7) | 25.0% (11.6-41.0) |
| MCC2 cohort | 23.9% (8.9-42.9) | 19.1% (6.1-37.7) | 9.6% (0.9-31.0) | n/a |
| High-risk | | | | |
| MCC1 cohort | 42.4% (30.6-53.6) | 26.7% (16.4-38.0) | 9.7% (2.9-21.4) | 9.7% (2.9-21.4) |
| MCC2 cohort | 41.3% (23.0-58.8) | 15.0% (4.7-30.8) | 3.8% (0.2-16.1) | n/a |
| Very-high-risk | | | | |
| MCC1 cohort | 15.7% (5.9-29.9) | 0% | 0% | 0% |
| MCC2 cohort | 11.1% (1.9-29.8) | 0% | 0% | 0% |

[a]Cells with "n/a" indicate all patients were censored prior to that specific time-point.

Supplementary Table 2. Univariable Cox regression analysis of overall survival for the clinical covariates.

| Clinical covariates | HR | *P* | 95% CI LL | 95% CI UL |
|---|---|---|---|---|
| Serum albumin, (g/dL) | 0.309466 | < .001 | 0.177733 | 0.538838 |
| Number of metastatic sites | 2.289917 | < .001 | 1.498369 | 3.499618 |
| Previous lines of therapy | 1.382078 | .007 | 1.093907 | 1.746162 |
| Neutrophils, (1e+9/L) | 1.054048 | .03 | 1.006576 | 1.103759 |
| WBC, (1e+9/L) | 1.035022 | .02 | 1.006785 | 1.064052 |
| ECOG | 1.666624 | .06 | 0.983612 | 2.823915 |
| Ratio of: Neutrophils/Lymphocytes | 1.028439 | .13 | 0.992106 | 1.066103 |
| Histology | 1.329578 | .22 | 0.845967 | 2.089653 |
| Sex | 0.784563 | .24 | 0.522821 | 1.177341 |
| Age at initiation of IO (65) | 1.220562 | .35 | 0.802604 | 1.856173 |
| *KRAS* mutational status | 0.774548 | .41 | 0.420311 | 1.427334 |
| *EGFR* mutational status | 0.909679 | .78 | 0.462681 | 1.788522 |
| Smoking status | 0.939899 | .81 | 0.567665 | 1.556216 |
| Lymphocytes | 1.004999 | .98 | 0.728651 | 1.386155 |
| Checkpoint inhibitor type | | | | |
| PD-1 *(reference)* | *1.00* | -- | -- | -- |
| PD-L1 | 1.19224 | .48 | 0.728812 | 1.950347 |
| Doublet | 0.6858804 | .15 | 0.4097269 | 1.14816 |
| Stage IV | 1.716386 | .36 | 0.5423838 | 5.431542 |

Supplementary Table 3. Univariable Cox regression analysis of overall survival for radiomic features that are stable and reproducible.

| Radiomic features[b] | HR | *P* | *P*[a] | 95% CI LL | 95% CI UL |
|---|---|---|---|---|---|
| **Group 1 features** | | | | | |
| GLCM inverse difference | 2.25402 | 5.8E-05 | .003 | 1.51689 | 3.34935 |
| Avg 3D RLN normalized (Run length non uniformity normalized) | 0.46097 | 5.9E-05 | .003 | 0.31597 | 0.67251 |
| GLCM inverse variance | 2.58076 | 7.7E-05 | .004 | 1.61319 | 4.12867 |
| Avg 3D SRE (Short runs emphasis) | 0.48066 | 8.1E-05 | .005 | 0.33389 | 0.69194 |
| Avg 3D RP (Run percentage) | 0.45772 | 9.1E-05 | .005 | 0.30948 | 0.67697 |
| GLSZM Zone percentage | 0.4052 | 0.0001 | .005 | 0.25672 | 0.63955 |
| Avg 3D LRE (Long runs emphasis) | 2.18298 | 0.00028 | .02 | 1.4321 | 3.32755 |
| Avg 3D RLV (Run length variance) | 2.7398 | 0.00031 | .02 | 1.584 | 4.73898 |
| Peritumoral Quartile coefficient of dispersion | 0.41027 | 0.00044 | .02 | 0.2496 | 0.67435 |
| Peritumoral Coefficient of variance | 0.46627 | 0.00093 | .05 | 0.29677 | 0.73256 |
| **Group 2 features** | | | | | |
| Peritumoral GLCM sum variance | 2.38627 | 0.00209 | .10 | 1.3713 | 4.15248 |
| Peritumoral GLCM cluster tendency | 2.38627 | 0.00209 | .10 | 1.3713 | 4.15248 |
| GLCM joint max | 2.21662 | 0.00211 | .10 | 1.33449 | 3.68185 |
| Peritumoral Volume at intensity fraction difference | 0.47749 | 0.00258 | .12 | 0.29526 | 0.7722 |
| Peritumoral GLCM Joint variance | 2.38808 | 0.00261 | .12 | 1.355 | 4.20878 |
| Peritumoral Statistical Median absolute deviation | 2.31779 | 0.0038 | .17 | 1.31186 | 4.09506 |
| Peritumoral Intensity histogram median absolute deviation | 2.31941 | 0.00385 | .17 | 1.31104 | 4.10336 |
| Peritumoral GLCM cluster prominence | 2.47459 | 0.00489 | .21 | 1.31658 | 4.65116 |
| Peritumoral mean absolute deviation | 2.21715 | 0.0057 | .23 | 1.26083 | 3.89883 |
| Peritumoral Volume at intensity fraction 10 | 0.50543 | 0.00577 | .23 | 0.31136 | 0.82047 |
| Peritumoral Intensity histogram mean absolute deviation | 2.21584 | 0.00578 | .23 | 1.25934 | 3.89882 |
| Peritumoral Avg 3D GV (Grey level variance) | 2.29666 | 0.00602 | .23 | 1.26885 | 4.15704 |
| Surface to volume ratio (mm2) | 0.45788 | 0.00632 | .23 | 0.26136 | 0.80215 |
| Peritumoral Avg 3D RE (Run entropy) | 2.04588 | 0.01262 | .45 | 1.16577 | 3.59045 |
| Peritumoral GLCM sum entropy | 2.05341 | 0.01359 | .48 | 1.15964 | 3.63606 |
| Peritumoral GLCM correlation | 1.67613 | 0.0163 | .55 | 1.09971 | 2.55466 |
| Peritumoral Intensity histogram entropy | 1.97162 | 0.01906 | .63 | 1.11772 | 3.47789 |
| Peritumoral Avg 3D GLN normalize (Grey level nonuniformity normalised) | 0.44736 | 0.023 | .74 | 0.22361 | 0.89502 |
| Peritumoral Intensity histogram uniformity | 0.45465 | 0.02442 | .75 | 0.22885 | 0.90325 |
| Peritumoral GLCM Joint Average | 1.70369 | 0.02875 | .86 | 1.05683 | 2.74647 |
| Peritumoral GLCM Sum average | 1.70369 | 0.02875 | .86 | 1.05683 | 2.74646 |
| GLCM first measure of information correlation | 0.50796 | 0.02909 | .83 | 0.27646 | 0.93332 |
| Peritumoral Minimum histogram gradient | 0.57727 | 0.03726 | 1.00605 | 0.34422 | 0.96809 |
| Peritumoral GLCM Joint entropy | 1.77844 | 0.04547 | 1.18226 | 1.01167 | 3.12638 |
| Peritumoral Intensity histogram quartile coefficient of dispersion | 1.79419 | 0.05237 | 1.30921 | 0.99403 | 3.23847 |
| Flatness | 0.60238 | 0.06022 | 1.4453 | 0.35504 | 1.02203 |
| Peritumoral GLSZM Zone size entropy | 1.80822 | 0.06067 | 1.4453 | 0.9738 | 3.35763 |

| | | | | | |
|---|---|---|---|---|---|
| GLSZM Small zone emphasis | 0.57098 | 0.075 | 1.64997 | 0.30811 | 1.05812 |
| Peritumoral Volume at intensity fraction 90 | 1.86338 | 0.09239 | 1.9402 | 0.90262 | 3.84682 |
| Peritumoral NGTDM Complexity | 1.62411 | 0.1312 | 2.62401 | 0.86522 | 3.04861 |
| Volume at intesity fraction 90 | 0.76203 | 0.27124 | 5.15362 | 0.46958 | 1.23661 |
| Volume at intesity fraction difference | 1.2654 | 0.34726 | 6.25067 | 0.77457 | 2.06726 |
| Peritumoral GLCM Difference variance | 1.28247 | 0.34929 | 6.25067 | 0.76171 | 2.15925 |
| Peritumoral Avg 3D LRE (Long runs emphasis) | 0.78181 | 0.40239 | 6.43829 | 0.43942 | 1.39097 |
| Peritumoral Avg 3D RP (Run percentage) | 1.24447 | 0.42946 | 6.44197 | 0.72337 | 2.14097 |
| Peritumoral Avg 3D RLV (Run length variance) | 0.80074 | 0.44286 | 6.44197 | 0.45394 | 1.41249 |
| Peritumoral GLCM Joint MAX | 0.81152 | 0.46754 | 6.20002 | 0.46196 | 1.4256 |
| GLSZM zone size non uniformity normalized | 0.7122 | 0.46993 | 6.07805 | 0.28366 | 1.78817 |
| Compactness | 0.83801 | 0.4855 | 5.63921 | 0.51 | 1.37698 |
| Peritumoral ENERGY | 1.22883 | 0.50817 | 5.3405 | 0.66744 | 2.26239 |
| Peritumoral Intensity at volume fraction 90 | 0.83603 | 0.54944 | 5.08168 | 0.46511 | 1.50274 |
| Peritumoral Intensity histogram coefficient of variance | 1.15359 | 0.61805 | 4.94493 | 0.65788 | 2.02281 |
| Energy | 1.25863 | 0.62224 | 4.94436 | 0.50406 | 3.14276 |
| Peritumoral GLSZM Low grey level zone emphasis | 0.90411 | 0.78368 | 4.70208 | 0.44023 | 1.85679 |
| Peritumoral NGTDM Coarseness | 0.91104 | 0.84024 | 4.70208 | 0.36826 | 2.25387 |
| Peritumoral Avg 3D LRLGE (Long run low grey level emphasis) | 1.02909 | 0.94955 | 4.20121 | 0.42334 | 2.50163 |
| Peritumoral NGTDM Busyness | 1.01946 | 0.95219 | 3.79819 | 0.54301 | 1.91395 |
| Peritumral Avg 3D RE (Run emphasis) | 1.0101 | 0.98034 | 2.85657 | 0.45414 | 2.24669 |
| Peritumoral Avg 3D SRLGE (Short run low grey level emphasis) | 1.0065 | 0.98681 | 1.96067 | 0.46668 | 2.17077 |
| | | | | | |
| **Group 3 features** | | | | | |
| Peritumoral Avg 3D RLN (Run length uniformity) | 1.00001 | 0.42852 | -- | 0.99998 | 1.00005 |
| Major Axis Length | 1.01174 | 0.00505 | -- | 1.00352 | 1.02003 |
| Longest Diameter | 1.00948 | 0.0053 | -- | 1.00281 | 1.01621 |
| Minor Axis Length | 1.01596 | 0.00601 | -- | 1.00455 | 1.0275 |
| Least Axis Length | 1.01555 | 0.04569 | -- | 1.0003 | 1.03104 |
| GLSZM Grey level non-uniformity | 1.00053 | 0.14298 | -- | 0.99982 | 1.00124 |
| Peritumoral GLSZM Zone size non-uniformity | 1.00007 | 0.34269 | -- | 0.99992 | 1.00022 |
| Peritumoral GLSZM Grey level non-uniformity | 1.00071 | 0.4389 | -- | 0.99892 | 1.00249 |

[a]*P* values are Bonferroni-Holm corrected. HR= hazard ratio; SE= standard error; LL= lower limit; UL= upper limit

[b]Group 1 features are significantly associated with overall survival, group 2 features are not significantly associated with survival, and group 3 features are highly correlated with tumor volume. Group 3 features were not included in the Bonferroni-Holm analyses.

Supplementary Table 4. Univariable and multivariable Cox regression analysis for overall survival for the VA cohort (N = 62)

| Overall survival | Univariable Model[a] HR (95% CI) | Multivariable Model[b] HR (95% CI) |
|---|---|---|
| Risk group[c] | | |
| Low-risk | *1.00 (Reference)* | *1.00 (Reference)* |
| Moderate-risk | 4.07 (0.90 – 18.26) | 4.00 (0.83 – 19.17) |
| High-risk | 4.72 (1.02 – 21.94) | 4.54 (0.90 – 23.11) |
| Very-high risk | 9.72 (2.08 – 45.49) | 13.81 (2.58 – 73.93) |
| Age | . | 1.00 (0.96 – 1.05) |
| Stage | . | 0.66 (0.23 – 1.93) |
| ECOG | . | 1.98 (0.99 – 3.94) |
| Lymphocytes | . | 1.13 (0.53 – 2.40) |
| NLR | . | 1.09 (0.99 – 1.18) |

Abbreviations: SD = standard deviation; HR = hazard ratio; CI = confidence interval; NLR = neutrophils to lymphocytes ratio

[a]The main effects for each risk group with the low risk group as the referent category.

[b]These models included the clinical covariates that were found to be significant different between the training and validation cohorts (Table 1) and the risk groups using the low risk group as the referent category.

[c]Low risk group refers to patients who have low GLCM inverse difference (≤0.43) and lower number of metastatic sites (1). The moderate risk group refers to patients who either have low GLCM inverse difference (≤0.43) and higher number of metastatic sites (≥2) or patients who have higher GLCM inverse difference (>0.43), higher serum albumin (≥3.9) and lower number of metastatic sites (1). The high-risk group refers to either patients who have higher GLCM inverse difference (>0.43), higher serum albumin (≥3.9) and higher number of metastatic sites (≥2) or patients who have higher GLCM inverse difference (>0.43), lower serum albumin (<3.9) and lower number of metastatic sites (1). The very-high-risk group refers to patients who have higher GLCM inverse difference (>0.43), lower serum albumin (<3.9) and lower number of metastatic sites (≥2).

Supplementary Table 5. Patient characteristics by CART risk groups[c] for the MCC1 cohort.

| Characteristic | Low-risk | Moderate-risk | High-risk | Very-high-risk | *P*[a] |
|---|---|---|---|---|---|
| Age at diagnosis, N (%) | | | | | |
| *Dichotomized* | | | | | |
| < 65 | 9 (42.9) | 22 (40.7) | 26 (37.1) | 11 (31.4) | |
| ≥ 65 | 12 (57.1) | 32 (59.3) | 44 (62.9) | 24 (68.6) | .79 |
| Sex, N (%) | | | | | |
| Female | 8 (38.1) | 31 (57.4) | 40 (57.1) | 16 (45.7) | |
| Male | 13 (61.9) | 23 (42.6) | 30 (42.9) | 19 (54.3) | .32 |
| Smoking status, N (%) | | | | | |
| Never smoker | 4 (19.1) | 10 (18.9) | 12 (17.9) | 4 (11.4) | |
| Ever smoker | 17 (80.9) | 43 (81.1) | 55 (82.1) | 31 (88.6) | .81 |
| Stage, N (%) | | | | | |
| III | 2 (9.5) | 0 (0) | 3 (4.3) | 1 (2.9) | |
| IV | 19 (90.5) | 54 (100) | 67 (95.7) | 34 (97.1) | .14 |
| Histology, N (%) | | | | | |
| Adenocarcinoma/others | 17 (81.0) | 43 (79.6) | 53 (75.7) | 24 (68.6) | |
| Squamous cell carcinoma | 4 (19.0) | 11 (20.4) | 17 (24.3) | 11 (31.4) | .64 |
| Checkpoint inhibitors, N (%) | | | | | |
| Anti PD-L1 | 4 (19.1) | 11 (20.37) | 24 (34.3) | 9 (25.7) | |
| Anti PD-1 | 7 (33.3) | 16 (29.6) | 25 (35.7) | 9 (25.7) | |
| Doublet | 10 (47.6) | 27 (50.0) | 21 (30.0) | 17 (48.6) | .29 |
| ECOG performance status, N (%) | | | | | |
| 0 | 10 (47.6) | 10 (18.5) | 15 (21.4) | 4 (11.4) | |
| 1 | 11 (52.4) | 44 (81.5) | 55 (78.6) | 31 (88.6) | .02 |
| Previous lines of therapy on current diagnosis, N (%) | | | | | |
| None | 10 (47.6) | 33 (61.1) | 10 (14.3) | 17 (48.6) | |
| 1 | 4 (19.1) | 13 (24.1) | 24 (34.3) | 7 (20.0) | |
| ≥ 2 | 7 (33.3) | 8 (14.8) | 36 (51.4) | 11 (31.4) | < .001 |
| Number of metastatic sites[b], N (%) | | | | | |
| 1 | 21 (100) | 14 (25.9) | 47 (67.1) | 0 (0) | |
| ≥ 2 | 0 (0) | 40 (74.1) | 23 (32.9) | 35 (100) | < .001 |
| *EGFR* mutational status, N (%) | | | | | |
| Not Detected | 14 (77.8) | 36 (87.8) | 37 (75.5) | 20 (83.3) | |
| Detected | 4 (22.2) | 5 (12.2) | 12 (24.5) | 4 (16.7) | .50 |
| *KRAS* mutational status, N (%) | | | | | |
| Not Detected | 7 (58.3) | 17 (60.7) | 26 (70.3) | 11 (84.6) | |
| Detected | 5 (41.7) | 11 (39.3) | 11 (29.7) | 2 (15.4) | .40 |
| Hematology, median, (95% CI) | | | | | |
| Serum albumin[b], (g/dL) | 4.0 (3.8-4.2) | 4.1 (4.1-4.2) | 4.0 (3.9-4.1) | 3.6 (3.5-3.7) | < .001 |
| Lymphocytes, (1e+9/L) | 1.0 (0.8-1.4) | 1.2 (1.2-1.4) | 1.4 (1.3-1.5) | 1.2 (0.8-1.6) | .22 |
| WBC, (1e+9/L) | 6.8 (5.1-8.8) | 6.9 (6.4-8.0) | 6.9 (6.4-7.4) | 8.3 (7.4-10.9) | .02 |
| Neutrophils, (1e+9/L) | 4.8 (3.7-6.4) | 4.7 (4.1-5.3) | 4.4 (3.9-4.9) | 6.1 (5.1-7.4) | .007 |
| Ratio of: Neutrophils/Lymphocytes | 4.1 (2.7-5.7) | 3.4 (2.8-4.0) | 3.1 (2.8-3.7) | 4.6 (3.8-7.0) | .004 |

Abbreviations:

[a]P values for continuous variables were calculated using Kruskall-Wallis test and Fisher's Exact Test of categorical variables. All tests were two-sided.

[b]Serum albumin and number of metastatic sites were not considered as potential confounders as these covariates were already part of the CART models. CI = confidence interval

[c]Low-risk group refers to patients who have low GLCM inverse difference (≤0.43) and lower number of metastatic sites (n=1). The moderate risk group refers to patients who either have low GLCM inverse difference (≤0.43) and higher number of metastatic sites (≥2) or patients who have higher GLCM inverse difference (>0.43), higher serum albumin (≥3.9) and lower number of metastatic sites (1). The high-risk group refers to either patients who have higher GLCM inverse difference (>0.43), higher serum albumin (≥3.9) and higher number of metastatic sites (≥2) or patients who have higher GLCM inverse difference (>0.43), lower serum albumin (<3.9) and lower number of metastatic sites (n=1). The very-high-risk group refers to patients who have higher GLCM inverse difference (>0.43), lower serum albumin (<3.9) and lower number of metastatic sites (≥2).

Supplementary Table 6. Multivariable model of radiomic features and clinical covariates that were significantly associated with OS in univariable analyses

| Radiomic Features | HR | *P* | 95% CI | |
|---|---|---|---|---|
| GLCM inverse difference | 1.23 | .03 | 1.03 | 1.47 |
| Peritumoral quartile coefficient of dispersion | 0.09 | .002 | 0.02 | 0.43 |
| Serum albumin, (g/dL) | 0.36 | .002 | 0.19 | 0.68 |
| Number of metastatic sites | 2.7 | < .001 | 1.72 | 4.26 |
| Previous lines of therapy | 1.45 | .007 | 1.11 | 1.89 |
| WBC (1e+9/L) | 0.99 | .85 | 0.91 | 1.08 |
| Neutrophils, (1e+9/L) | 1.02 | 0.79 | 0.89 | 1.16 |

| Supplementary Table 7. Gene list for statistically significant probes | | | | | | |
|---|---|---|---|---|---|---|
| Probeset | *P* | Log2 Ratio (High GLCM - Low GLCM) | Correlation Coefficient | Symbol | Location | Description |
| merck-NM_001216_at | 1.32E-05 | 1.370676338 | 0.439478749 | CA9 | 9p13.3 | carbonic anhydrase 9 |
| merck2-DQ892208_at | 2.49E-05 | 1.250844271 | 0.433548156 | CA9 | 9p13.3 | carbonic anhydrase 9 |
| merck-NM_138435_at | 0.000522015 | 0.621354657 | 0.408057524 | FAM83F | 22q13.1 | family with sequence similarity 83 member F |
| merck2-BC052608_at | 0.000601472 | -1.14810035 | -0.400142163 | TYRP1 | 9p23 | tyrosinase related protein 1 |
| merck2-BC065305_at | 0.000129621 | -1.16182618 | -0.400529687 | C7 | 5p13.1 | complement C7 |
| merck-NM_001009567_s_at | 0.0005668 | -0.505840657 | -0.400805476 | MRC1 | 10p12.33 | mannose receptor C-type 1 |
| merck-NM_153264_s_at | 8.23E-05 | -1.207502221 | -0.401264345 | COL6A5 | 3q22.1 | collagen type VI alpha 5 chain |
| merck-AK092659_at | 5.61E-05 | -0.665885655 | -0.401815358 | SHROOM4 | Xp11.22 | shroom family member 4 |
| merck2-AJ515553_at | 0.000143828 | -0.581436069 | -0.402041333 | JAML | 11q23.3 | junction adhesion molecule like |
| merck-NM_004165_at | 2.38E-05 | -0.931657378 | -0.402299785 | RRAD | 16q22.1 | RRAD |
| merck-ENST00000370678_s_at | 8.26E-06 | -0.63811276 | -0.402452885 | FHL1 | Xq26.3 | four and a half LIM domains 1 |
| merck-NM_001449_at | 3.15E-06 | -0.976777977 | -0.403268835 | FHL1 | Xq26.3 | four and a half LIM domains 1 |
| merck2-BX648828_at | 1.83E-05 | -0.943935929 | -0.40361099 | ROBO2 | 3p12.3 | roundabout guidance receptor 2 |
| merck-NM_198098_at | 0.000668776 | -0.669061462 | -0.403640886 | AQP1 | 7p14.3 | aquaporin 1 (Colton blood group) |
| merck2-BC050635_at | 6.08E-05 | -0.754311143 | -0.403710847 | CELF2 | 10p14 | CUGBP Elav-like family member 2 |
| merck-AF077048_a_at | 7.66E-05 | -0.560297305 | -0.404203317 | SSBP2 | 5q14.1 | single stranded DNA binding protein 2 |
| merck-AK123737_s_at | 4.98E-05 | -0.946965722 | -0.404803204 | ABI3BP | 3q12.2 | ABI family member 3 binding protein |
| merck-AK091353_at | 0.000364347 | -0.618962068 | -0.405158937 | NUDT16 | 3q22.1 | nudix hydrolase 16 |
| merck-NM_015717_at | 0.000804365 | -1.258808138 | -0.40528679 | CD207 | 2p13.3 | CD207 molecule |
| merck-NM_000231_at | 0.000169064 | -0.874940131 | -0.405591591 | SGCG | 13q12.12 | sarcoglycan gamma |
| merck2-NM_004657_at | 1.21E-05 | -1.111171997 | -0.405621821 | SDPR | 2q32.3 | serum deprivation response |
| merck-NM_003018_s_at | 0.000833713 | -2.146148608 | -0.405772801 | SFTPC | 8p21.3 | surfactant protein C |
| merck- | 0.000183147 | -0.607781977 | -0.406283628 | CAV2 | 7q31.2 | caveolin 2 |

| | | | | | | |
|---|---|---|---|---|---|---|
| NM_001233_at | | | | | | |
| merck-NM_006774_at | 3.50E-05 | -1.096470411 | -0.40702071 | INMT | 7p14.3 | indolethylamine N-methyltransferase |
| merck-NM_003956_at | 2.66E-05 | -1.117257052 | -0.407471565 | CH25H | 10q23.31 | cholesterol 25-hydroxylase |
| merck-NM_198392_at | 7.04E-06 | -1.465595101 | -0.407583914 | TCF21 | 6q23.2 | transcription factor 21 |
| merck-NM_030820_at | 0.000101006 | -1.108105019 | -0.407880565 | COL21A1 | 6p12.1\|6p12.3-p11.2 | collagen type XXI alpha 1 chain |
| merck-ENST00000368557_at | 7.55E-06 | -0.95478475 | -0.408531546 | FAM162B | 6q22.1 | family with sequence similarity 162 member B |
| merck-NM_032609_s_at | 3.10E-06 | -0.993974659 | -0.408770739 | COX4I2 | 20q11.21 | cytochrome c oxidase subunit 4I2 |
| merck2-BM555890_a_at | 1.54E-05 | -1.065187208 | -0.409387768 | SDPR | 2q32.3 | serum deprivation response |
| merck-NM_000316_at | 0.000802569 | -0.554507482 | -0.410011189 | PTH1R | 3p21.31 | parathyroid hormone 1 receptor |
| merck-AK090694_at | 4.38E-05 | -0.693074069 | -0.410126842 | ZNF366 | 5q13.2\|5q13.2 | zinc finger protein 366 |
| merck2-NM_005264_at | 0.000539411 | -0.738028013 | -0.410217178 | GFRA1 | 10q25.3 | GDNF family receptor alpha 1 |
| merck-NM_031911_a_at | 0.000174311 | -1.105796271 | -0.410718695 | C1QTNF7 | 4p15.32 | C1q and TNF related 7 |
| merck-NM_153206_s_at | 0.000197602 | -0.559129987 | -0.411070457 | JAML | 11q23.3 | junction adhesion molecule like |
| merck2-Z26653_at | 0.000305672 | -0.564899229 | -0.41193139 | LAMA2 | 6q22.33 | laminin subunit alpha 2 |
| merck-AF074993_at | 6.96E-06 | -0.571877851 | -0.412045353 | CAV1 | 7q31.2 | caveolin 1 |
| merck-AK055621_at | 0.000219429 | -0.889372602 | -0.412414835 | LINC00968 | 8q12.1 | long intergenic non-protein coding RNA 968 |
| merck-NM_001753_at | 5.72E-06 | -0.630940993 | -0.412502185 | CAV1 | 7q31.2 | caveolin 1 |
| merck-NM_030964_s_at | 9.38E-05 | -0.612566723 | -0.412609943 | SPRY4 | 5q31.3 | sprouty RTK signaling antagonist 4 |
| merck-AK093713_at | 4.83E-06 | -0.906997129 | -0.412839223 | --- | --- | --- |
| merck-NM_001035_a_at | 1.77E-06 | -0.942099651 | -0.416588769 | RYR2 | 1q43 | ryanodine receptor 2 |
| merck2-EB387139_a_at | 1.12E-05 | -1.045611921 | -0.418330623 | ATP1A2 | 1q23.2 | ATPase Na+/K+ transporting subunit alpha 2 |
| merck-NM_014917_at | 4.80E-06 | -1.074865523 | -0.41874915 | NTNG1 | 1p13.3 | netrin G1 |
| merck2-NM_006774_at | 1.84E-05 | -1.147417221 | -0.418770379 | INMT | 7p14.3 | indolethylamine N-methyltransferase |
| merck-HSS00001975_s_at | 1.33E-05 | -0.555345671 | -0.420548137 | LOC101928304 | 6q23.2 | uncharacterized LOC101928304 |
| merck-NM_002404_at | 4.87E-05 | -0.79518393 | -0.420697232 | MFAP4 | 17p11.2 | microfibrillar associated protein 4 |

| | | | | | | |
|---|---|---|---|---|---|---|
| merck-NM_003206_a_at | 6.39E-07 | -1.256723496 | -0.420972884 | TCF21 | 6q23.2 | transcription factor 21 |
| merck-NM_000139_at | 0.000759594 | -0.896722186 | -0.421165414 | MS4A2 | 11q12.1 | membrane spanning 4-domains A2 |
| merck-NM_022062_s_at | 4.34E-07 | -0.827394611 | -0.421219534 | PKNOX2 | 11q24.2 | PBX/knotted 1 homeobox 2 |
| merck-NM_003189_at | 1.71E-06 | -0.823409424 | -0.421281907 | TAL1 | 1p33 | TAL bHLH transcription factor 1, erythroid differentiation factor |
| merck-AK057197_a_at | 0.000112885 | -1.582948367 | -0.421358494 | PRG4 | 1q31.1 | proteoglycan 4 |
| merck-NM_000426_at | 0.000227964 | -0.586936306 | -0.4224352 | LAMA2 | 6q22.33 | laminin subunit alpha 2 |
| merck2-AL832100_at | 0.000117353 | -0.554763515 | -0.422497317 | ZNF540 | 19q13.12 | zinc finger protein 540 |
| merck-AY102069_at | 0.000146733 | -1.344709354 | -0.422630104 | SFTA1P | 10p14 | surfactant associated 1, pseudogene |
| merck-BC039203_at | 7.60E-05 | -0.587628672 | -0.423279126 | RAPGEF5 | 7p15.3 | Rap guanine nucleotide exchange factor 5 |
| merck2-BC062365_at | 5.42E-05 | -0.942233186 | -0.423444816 | SLIT3 | 5q34-q35.1 | slit guidance ligand 3 |
| merck-NM_212464_s_at | 7.97E-06 | -0.712560384 | -0.423771173 | CAPN3 | 15q15.1 | calpain 3 |
| merck-BX648964_at | 0.000381206 | -1.175392198 | -0.423981709 | GFRA1 | 10q25.3 | GDNF family receptor alpha 1 |
| merck-NM_152606_at | 0.000298447 | -0.698250628 | -0.425139456 | ZNF540 | 19q13.12 | zinc finger protein 540 |
| merck-AK123264_at | 1.88E-05 | -0.891514948 | -0.425996926 | C1orf132 | 1q32.2 | chromosome 1 open reading frame 132 |
| merck-BU681386_at | 2.76E-06 | -1.558515379 | -0.426107186 | SCN7A | 2q24.3 | sodium voltage-gated channel alpha subunit 7 |
| merck2-CB240565_at | 1.53E-05 | -0.717460833 | -0.426664568 | GANC | 15q15.1 | glucosidase alpha, neutral C |
| merck-NM_174934_at | 6.67E-06 | -0.943362036 | -0.426758185 | SCN4B | 11q23.3 | sodium voltage-gated channel beta subunit 4 |
| merck-NM_002084_at | 3.43E-06 | -0.771043271 | -0.427463786 | GPX3 | 5q33.1 | glutathione peroxidase 3 |
| merck-NM_018488_at | 7.56E-06 | -0.88784239 | -0.427639025 | TBX4 | 17q23.2 | T-box 4 |
| merck-AL133118_at | 7.58E-06 | -1.085830953 | -0.428022321 | EMCN | 4q24 | endomucin |
| merck-AK074308_at | 6.77E-05 | -0.971112662 | -0.428367285 | ART4 | 12p12.3 | ADP-ribosyltransferase 4 (Dombrock blood group) |
| merck- | 0.000237851 | -0.547434758 | -0.428515485 | TMEM243 | 7q21.12 | transmembrane |

| | | | | | | |
|---|---|---|---|---|---|---|
| NM_024315_at | | | | | | protein 243 |
| merck-NM_153267_at | 1.50E-05 | -1.481129251 | -0.429033119 | MAMDC2 | 9q21.12 | MAM domain containing 2 |
| merck2-BC021053_at | 0.000265327 | -0.804390544 | -0.429755873 | SELENOP | 5p12 | selenoprotein P |
| merck-NM_021902_s_at | 5.78E-05 | -0.943043399 | -0.430648796 | FXYD1 | 19q13.12 | FXYD domain containing ion transport regulator 1 |
| merck-BX106890_a_at | 9.05E-06 | -1.063343772 | -0.431307083 | ITGA8 | 10p13 | integrin subunit alpha 8 |
| merck2-NG_001111_s_at | 0.000100391 | -1.078026891 | -0.431685313 | CYP21A2 | 6p21.33 | cytochrome P450 family 21 subfamily A member 2 |
| merck2-AI478811_at | 5.32E-06 | -1.135784076 | -0.431808963 | EMCN | 4q24 | endomucin |
| merck-AK057923_at | 1.96E-06 | -1.02717316 | -0.432254395 | ADAMTS9-AS2 | 3p14.1 | ADAMTS9 antisense RNA 2 |
| merck-NM_001870_at | 0.000687921 | -0.873028541 | -0.432337314 | CPA3 | 3q24 | carboxypeptidase A3 |
| merck-AL834346_at | 1.24E-05 | -1.269938187 | -0.433030705 | STXBP6 | 14q12 | syntaxin binding protein 6 |
| merck-NM_002942_at | 6.56E-05 | -1.512198445 | -0.433032352 | ROBO2 | 3p12.3 | roundabout guidance receptor 2 |
| merck-NM_004962_at | 8.33E-06 | -1.470970464 | -0.43376457 | GDF10 | 10q11.22 | growth differentiation factor 10 |
| merck-NM_015215_at | 0.000517422 | -0.832668783 | -0.434041057 | CAMTA1 | 1p36.31-p36.23 | calmodulin binding transcription activator 1 |
| merck-AK058175_a_at | 4.66E-06 | -0.856094267 | -0.434194991 | FHL5 | 6q16.1 | four and a half LIM domains 5 |
| merck-NM_004484_at | 7.79E-06 | -1.073685005 | -0.434742986 | GPC3 | Xq26.2 | glypican 3 |
| merck-NM_152765_s_at | 5.81E-05 | -0.723117859 | -0.435866312 | C8orf46 | 8q13.1 | chromosome 8 open reading frame 46 |
| merck2-BC142620_at | 8.78E-06 | -1.19675256 | -0.436106626 | TBX4 | 17q23.2 | T-box 4 |
| merck2-AV653866_at | 0.000107965 | -1.595989074 | -0.438897535 | ADH1B | 4q23 | alcohol dehydrogenase 1B (class I), beta polypeptide |
| merck2-NM_152547_at | 4.83E-07 | -1.701825785 | -0.440036633 | BTNL9 | 5q35.3 | butyrophilin like 9 |
| merck2-AL831991_at | 1.83E-06 | -1.343723391 | -0.440136541 | ATP1A2 | 1q23.2 | ATPase Na+/K+ transporting subunit alpha 2 |
| merck-NM_003638_a_at | 1.48E-05 | -1.018309335 | -0.442618163 | ITGA8 | 10p13 | integrin subunit alpha 8 |
| merck-NM_058240_s_at | 3.08E-05 | -0.839862119 | -0.444406373 | SLC8A3 | 14q24.2 | solute carrier family 8 member A3 |
| merck-CD700286_s_at | 7.18E-05 | -1.707753629 | -0.449985967 | ADH1B | 4q23 | alcohol dehydrogenase 1B |

| | | | | | | |
|---|---|---|---|---|---|---|
| | | | | | | (class I), beta polypeptide |
| merck-NM_152547_s_at | 7.01E-07 | -1.685132055 | -0.4504326 | BTNL9 | 5q35.3 | butyrophilin like 9 |
| merck2-X03350_at | 0.00011975 | -1.673130597 | -0.451055184 | ADH1B | 4q23 | alcohol dehydrogenase 1B (class I), beta polypeptide |
| merck-ENST00000375247_a_at | 9.91E-05 | -0.955407969 | -0.451579506 | TNXB | 6p21.33-p21.32 | tenascin XB |
| merck2-AK092282_at | 1.19E-05 | -0.84235733 | -0.452254129 | TM4SF18 | 3q25.1 | transmembrane 4 L six family member 18 |
| merck-ENST00000378076_at | 2.24E-05 | -1.010155062 | -0.45243341 | ITGA8 | 10p13 | integrin subunit alpha 8 |
| merck-NM_016438_at | 5.68E-08 | -1.081742653 | -0.452722602 | HIGD1B | 17q21.31 | HIG1 hypoxia inducible domain family member 1B |
| merck2-NM_000500_at | 0.000108697 | -1.085759757 | -0.453248691 | CYP21A2 | 6p21.33 | cytochrome P450 family 21 subfamily A member 2 |
| merck2-BC047725_at | 2.33E-05 | -0.998553607 | -0.456631723 | MFAP4 | 17p11.2 | microfibrillar associated protein 4 |
| merck2-ABV60894_at | 3.02E-05 | -1.521755032 | -0.45756447 | --- | --- | --- |
| merck-NM_001452_at | 2.09E-05 | -0.758237842 | -0.457710072 | FOXF2 | 6p25.3 | forkhead box F2 |
| merck2-NM_014485_at | 8.37E-05 | -0.964111203 | -0.458292656 | HPGDS | 4q22.3 | hematopoietic prostaglandin D synthase |
| merck-NM_018334_at | 1.16E-05 | -1.12425379 | -0.458857073 | LRRN3 | 7q31.1 | leucine rich repeat neuronal 3 |
| merck-ENST00000298441_a_at | 6.61E-06 | -1.200919933 | -0.461301197 | ITIH5 | 10p14 | inter-alpha-trypsin inhibitor heavy chain family member 5 |
| merck2-NM_019105_at | 4.04E-05 | -1.005138039 | -0.463323093 | TNXB | 6p21.33-p21.32 | tenascin XB |
| merck-BX647469_a_at | 5.18E-05 | -1.803332146 | -0.465262841 | ADH1B | 4q23 | alcohol dehydrogenase 1B (class I), beta polypeptide |
| merck-NM_018286_at | 3.02E-06 | -1.613847131 | -0.468823039 | TMEM100 | 17q22 | transmembrane protein 100 |
| merck2-AI620331_at | 0.000436108 | -0.699287666 | -0.46934759 | CFD | 19p13.3 | complement factor D |
| merck-NM_007037_at | 2.99E-05 | -1.345310481 | -0.471578735 | ADAMTS8 | 11q24.3 | ADAM metallopeptidase with thrombospondin type 1 motif 8 |
| merck- | 6.62E-05 | -0.988050389 | -0.473135606 | HPGDS | 4q22.3 | hematopoietic |

| | | | | | | |
|---|---|---|---|---|---|---|
| BC020734_a_at | | | | | | prostaglandin D synthase |
| merck2-AK095175_at | 2.38E-06 | -1.736491019 | -0.474890237 | TMEM100 | 17q22 | transmembrane protein 100 |
| merck2-BC057807_at | 3.54E-05 | -0.846869648 | -0.476359552 | CFD | 19p13.3 | complement factor D |
| merck2-AK027375_at | 7.29E-07 | -1.239488868 | -0.479279361 | ITIH5 | 10p14 | inter-alpha-trypsin inhibitor heavy chain family member 5 |
| merck-NM_002001_at | 3.63E-05 | -1.321088694 | -0.480942825 | FCER1A | 1q23.2 | Fc fragment of IgE receptor Ia |
| merck-NM_030569_at | 2.93E-07 | -1.392536082 | -0.481247896 | ITIH5 | 10p14 | inter-alpha-trypsin inhibitor heavy chain family member 5 |
| merck2-BI597924_at | 1.51E-07 | -0.857341242 | -0.486209534 | RGCC | 13q14.11 | regulator of cell cycle |
| merck2-NM_020482_at | 6.37E-07 | -1.26649873 | -0.491293697 | FHL5 | 6q16.1 | four and a half LIM domains 5 |
| merck-NM_014279_at | 0.000746598 | -0.82623735 | -0.492027847 | OLFM1 | 9q34.3 | olfactomedin 1 |
| merck-NM_001007544_at | 3.07E-05 | -1.164078018 | -0.499238556 | C1orf186 | 1q32.1 | chromosome 1 open reading frame 186 |
| merck-NM_014059_s_at | 9.59E-08 | -0.91803703 | -0.499821141 | RGCC | 13q14.11 | regulator of cell cycle |
| merck-NM_001765_at | 8.79E-06 | -1.053206977 | -0.505355871 | CD1C | 1q23.1 | CD1c molecule |
| merck-NM_004469_at | 3.30E-07 | -2.185856675 | -0.506521247 | VEGFD PIR-FIGF | Xp22.2 | vascular endothelial growth factor D \|\|\| PIR-FIGF readthrough |
| merck2-AK226024_at | 8.20E-06 | -1.089628741 | -0.508387798 | CD1C | 1q23.1 | CD1c molecule |

| Supplementary Table 8. The radiomics quality score (RQS) | | |
|---|---|---|
| Criteria | Points system | Study point |
| Image protocol quality - well-documented image protocols (for example, contrast, slice thickness, energy, etc.) and/or usage of public image protocols allow reproducibility/replicability | + 1 (if protocols are well-documented) + 1 (if public protocol is used) | 2 |
| Multiple segmentations - possible actions are: segmentation by different physicians/algorithms/software, perturbing segmentations by (random) noise, segmentation at different breathing cycles. Analyse feature robustness to segmentation variabilities | 1 | 1 |
| Phantom study on all scanners - detect inter-scanner differences and vendor-dependent features. Analyse feature robustness to these sources of variability | 1 | 0 |
| Imaging at multiple time points - collect images of individuals at additional time points. Analyse feature robustness to temporal variabilities (for example, organ movement, organ expansion/shrinkage) | 1 | 1 |
| Feature reduction or adjustment for multiple testing - decreases the risk of overfitting. Overfitting is inevitable if the number of features exceeds the number of samples. Consider feature robustness when selecting features | − 3 (if neither measure is implemented) + 3 (if either measure is implemented) | 3 |
| Multivariable analysis with non radiomics features (for example, EGFR mutation) - is expected to provide a more holistic model. Permits correlating/inferencing between radiomics and non radiomics features | 1 | 1 |
| Detect and discuss biological correlates - demonstration of phenotypic differences (possibly associated with underlying gene–protein expression patterns) deepens understanding of radiomics and biology | 1 | 1 |
| Cut-off analyses - determine risk groups by either the median, a previously published cut-off or report a continuous risk variable. Reduces the risk of reporting overly optimistic results | 1 | 1 |
| Discrimination statistics - report discrimination statistics (for example, C-statistic, ROC curve, AUC) and their statistical significance (for example, p-values, confidence intervals). One can also apply resampling method (for example, bootstrapping, cross-validation) | + 1 (if a discrimination statistic and its statistical significance are reported) + 1 (if a resampling method technique is also applied) | 1 |
| Calibration statistics - report calibration statistics (for example, Calibration-in-the-large/slope, calibration plots) and their statistical significance (for example, *P*-values, confidence intervals). One can also apply resampling method (for example, bootstrapping, cross-validation) | + 1 (if a calibration statistic and its statistical significance are reported) + 1 (if a resampling method technique is also applied) | 0 |
| Prospective study registered in a trial database - provides the highest level of evidence supporting the clinical validity and usefulness of the radiomics biomarker | + 7 (for prospective validation of a radiomics signature in an appropriate trial) | 0 |

| | | |
|---|---|---|
| Validation - the validation is performed without retraining and without adaptation of the cut-off value, provides crucial information with regard to credible clinical performance | - 5 (if validation is missing) + 2 (if validation is based on a dataset from the same institute) + 3 (if validation is based on a dataset from another institute) + 4 (if validation is based on two datasets from two distinct institutes) + 4 (if the study validates a previously published signature) + 5 (if validation is based on three or more datasets from distinct institutes) | 5* |
| Comparison to 'gold standard' - assess the extent to which the model agrees with/is superior to the current 'gold standard' method (for example, TNM-staging for survival prediction). This comparison shows the added value of radiomics | 2 | 2 |
| Potential clinical utility - report on the current and potential application of the model in a clinical setting (for example, decision curve analysis) | 2 | 2 |
| Cost-effectiveness analysis - report on the cost-effectiveness of the clinical application (for example, QALYs generated) | 1 | 0 |
| Open science and data - make code and data publicly available. Open science facilitates knowledge transfer and reproducibility of the study | + 1 (if scans are open source) + 1 (if region of interest segmentations are open source) + 1 (if code is open source) + 1 (if radiomics features are calculated on a set of representative ROIs and the calculated features and representative ROIs are open source) | 2** |
| | | 22/36 score |

Supplementary Table 9. Clinical covariates by image feature GLCM inverse difference in the training cohort

| | GLCM inverse difference Training cohort | | |
|---|---|---|---|
| Clinical covariate | LOW | HIGH | *P*[a] |
| Age at immunotherapy baseline, N (%) | | | |
| < 65 | 20 (44.4) | 48 (35.6) | .29 |
| ≥ 65 | 25 (55.6) | 87 (64.4) | |
| Gender, N (%) | | | |
| Female | 21 (46.7) | 74 (54.8) | .39 |
| Male | 24 (53.3) | 61 (45.2) | |
| Smoking status[1] | | | |
| Never smokers | 8 (18.2) | 22 (16.7) | .82 |
| Ever smokers | 36 (81.8) | 110 (83.3) | |
| Unknown/Missing | | | |
| Stage, N (%) | | | |
| III | 2 (4.4) | 4 (3.0) | .64 |
| IV | 43 (95.6) | 131 (97.0) | |
| ECOG performance status, N (%) | | | |
| 0 | 15 (3.3) | 24 (17.8) | .04 |
| 1 | 30 (66.7) | 111 (82.2) | |
| 2 | 0 (0) | 0 (0) | |
| Previous lines of therapy on current diagnosis | | | |
| None | 19 (42.2) | 51 (37.8) | .82 |
| 1 | 12 (26.7) | 36 (26.7) | |
| ≥ 2 | 14 (31.1) | 48 (35.6) | |
| Number of metastatic sites | | | |
| 1 to 2 | 3 (8.6) | 3 (25.0) | .87 |
| ≥ 3 | 1 (2.9) | 3 (25.0) | |
| EGFR mutational status[1] | | | |
| Not Detected | 30 (85.7) | 77 (79.4) | .46 |
| Detected | 5 (14.3) | 20 (20.6) | |
| KRAS mutational status[1] | | | |
| Not Detected | 16 (64.0) | 45 (69.2) | .63 |
| Detected | 9 (36.0) | 20 (30.8) | |
| Hematology, median, (Range) | | | |
| Serum albumin, (g/dL) | 4.0 (3.1-47) | 4.0 (2.8-4.9) | .19 |
| Lymphocytes, (1e+9/L) | 1.2 (0.5-2.7) | 1.3 (0.3-3.7) | .15 |
| WBC, (1e+9/L) | 6.5 (0.5-2.7) | 7.2 (0.3-3.6) | .24 |

| | | | |
|---|---|---|---|
| Neutrophils, (1e+9/L) | 4.8 (3.7-16.8) | 4.7 (3.2-61.5) | .38 |
| Ratio of: Neutrophils/Lymphocytes | 3.7 (1.2-26.0) | 3.7 (1.1-30.4 | .89 |

Abbreviations: CI = confidence interval; NLR = neutrophils to lymphocytes ratio;
[a]*P* values for Smoking status, EGFR mutational status and KRAS mutational status were calculated for patients without missing/inconclusive data. *P* values for continuous variables were calculated using Mann-Whitney test and Fisher's Exact Test of categorical variables.

## Supplementary Figures

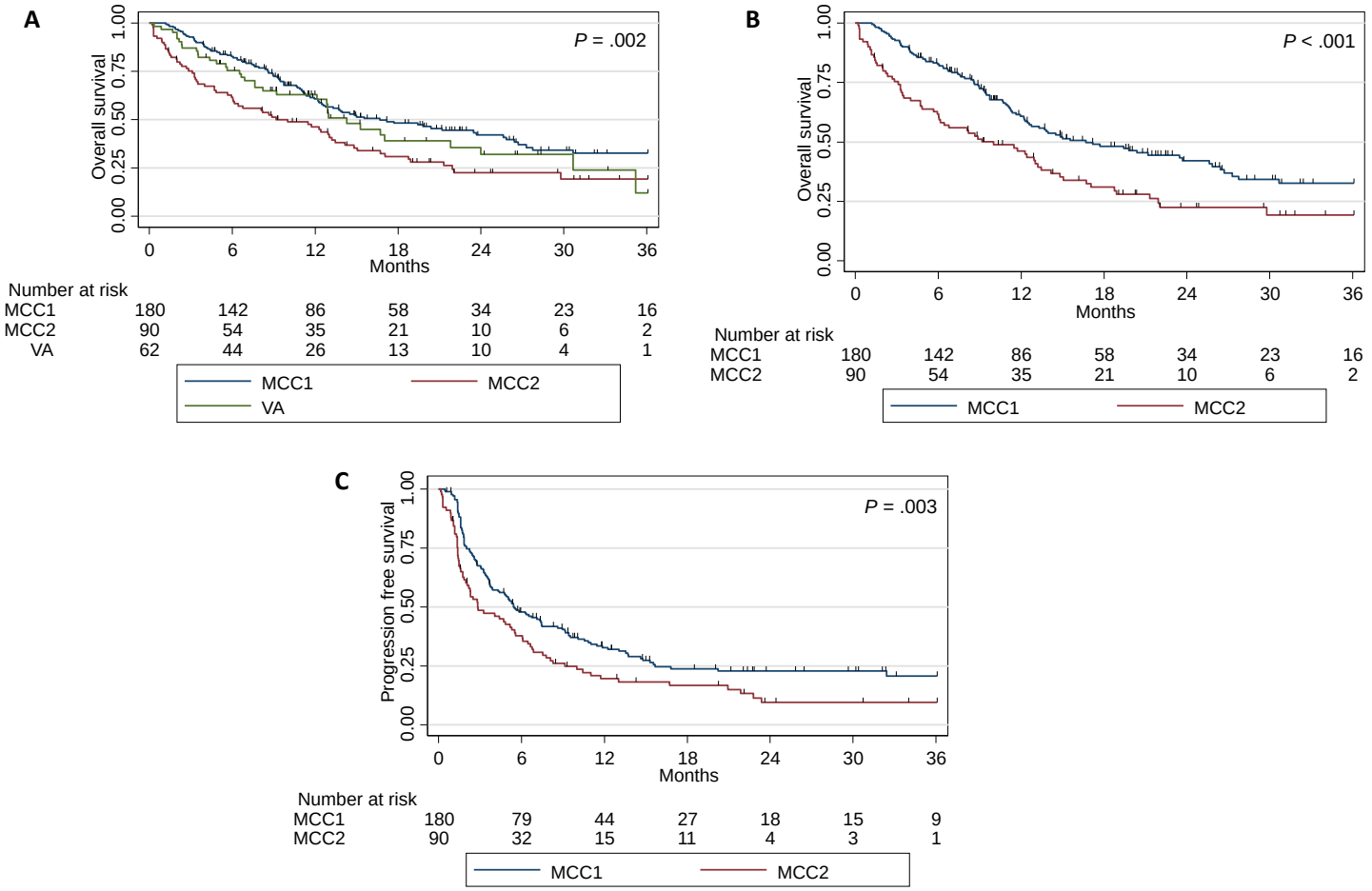


**Supplementary Figure 1**. **Kaplan-Meier survival curves for the MCC1 (training), MCC2 (test), and VA (validation) cohorts. A)** Overall survival for the MCC1, MCC2, and VA cohorts. **B)** Overall survival for the MCC1 and MCC2 cohorts. **C)** Progression-free survival for the MCC1 and MCC2 cohorts. PFS was not available for the VA cohort.

## TRAINING COHORT

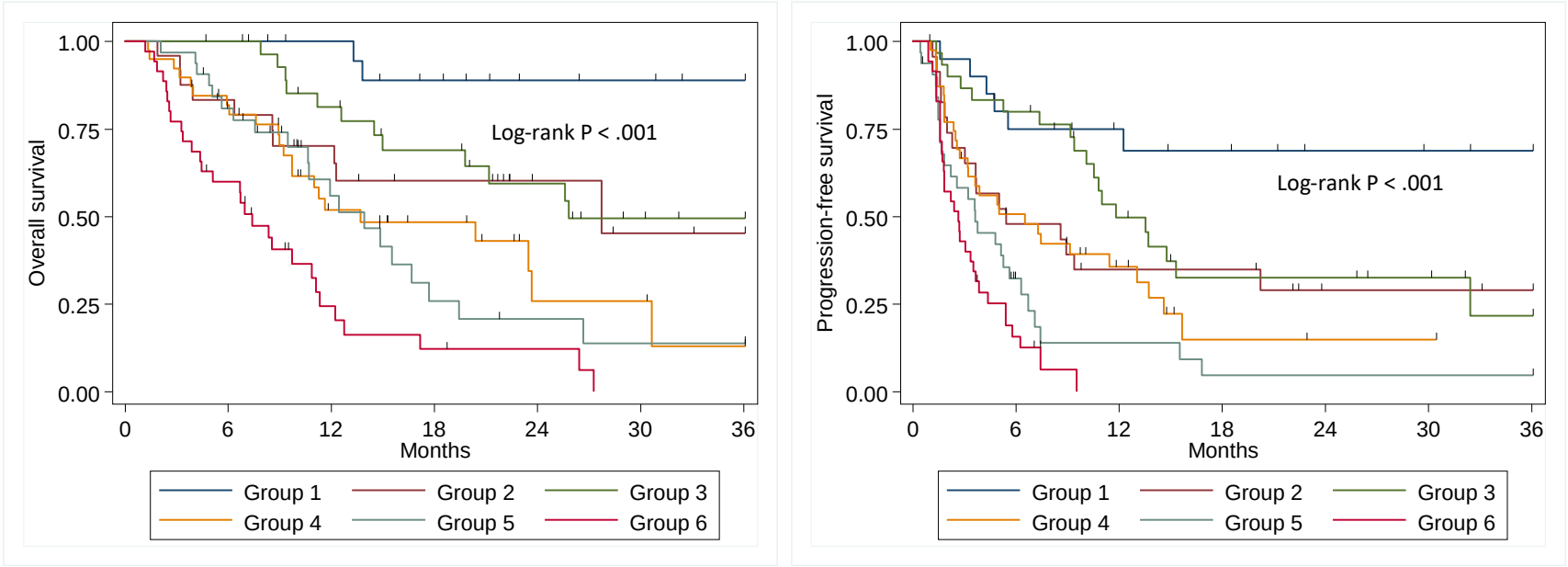


**Supplementary Figure 2**. **Overall survival and progression-free survival for the six risk groups identified by CART in the training cohort.** Groups 2 and 3 and groups 4 and 5 were combined for the subsequent analyses.

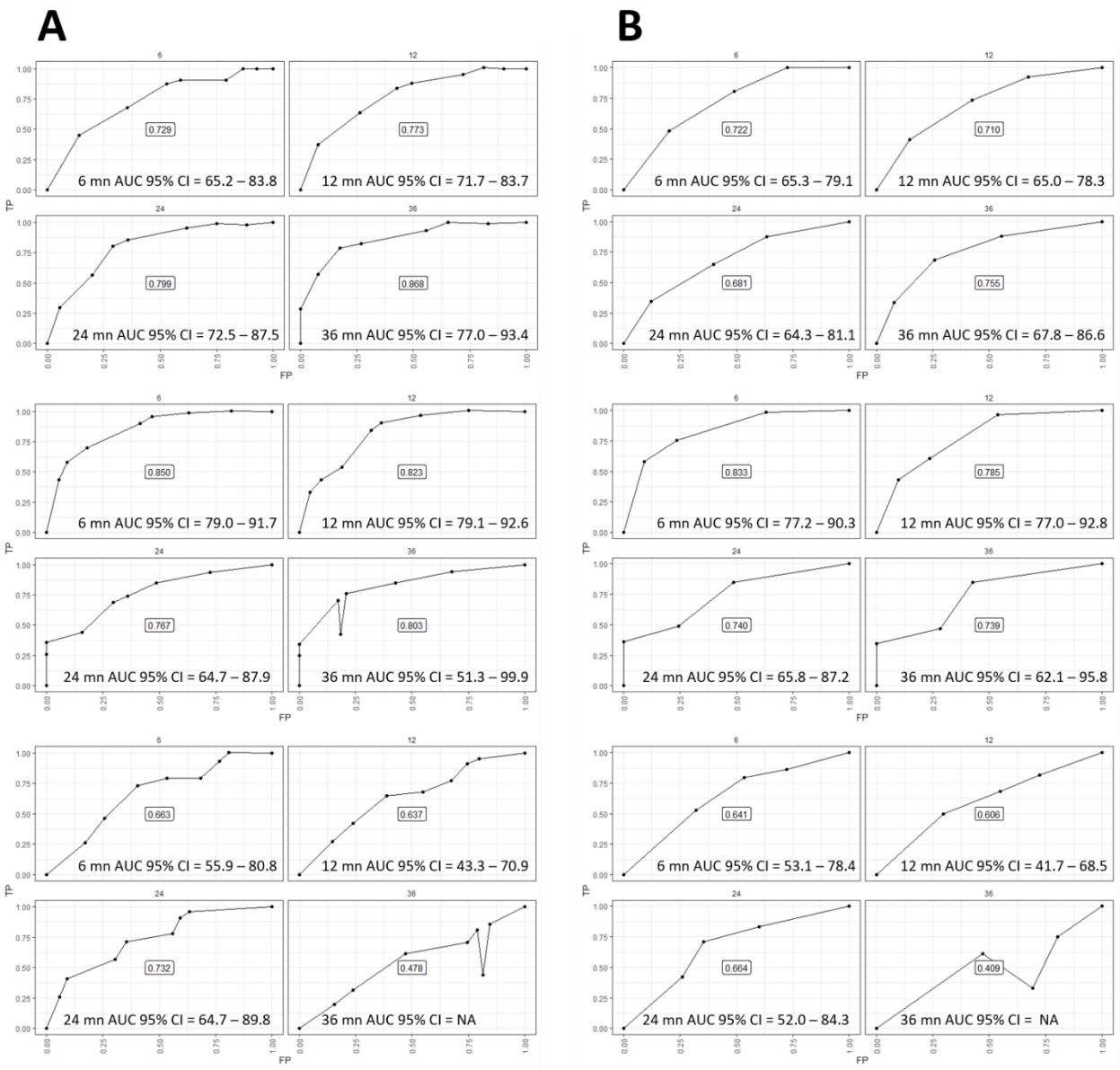


**Supplementary Figure 3**. **Time-dependent AUC curves for Cox regression models based on 6, 12, 24 and 36 months for training (top), test (middle) and validation cohorts (bottom). A)** AUCs for the final model that included 2 clinical and 1 radiomic feature. **B)** AUCs for the model with only 2 clinical features. All features and clinical covariates included were dichotomized by novel cut-points found by CART. (mn = months)

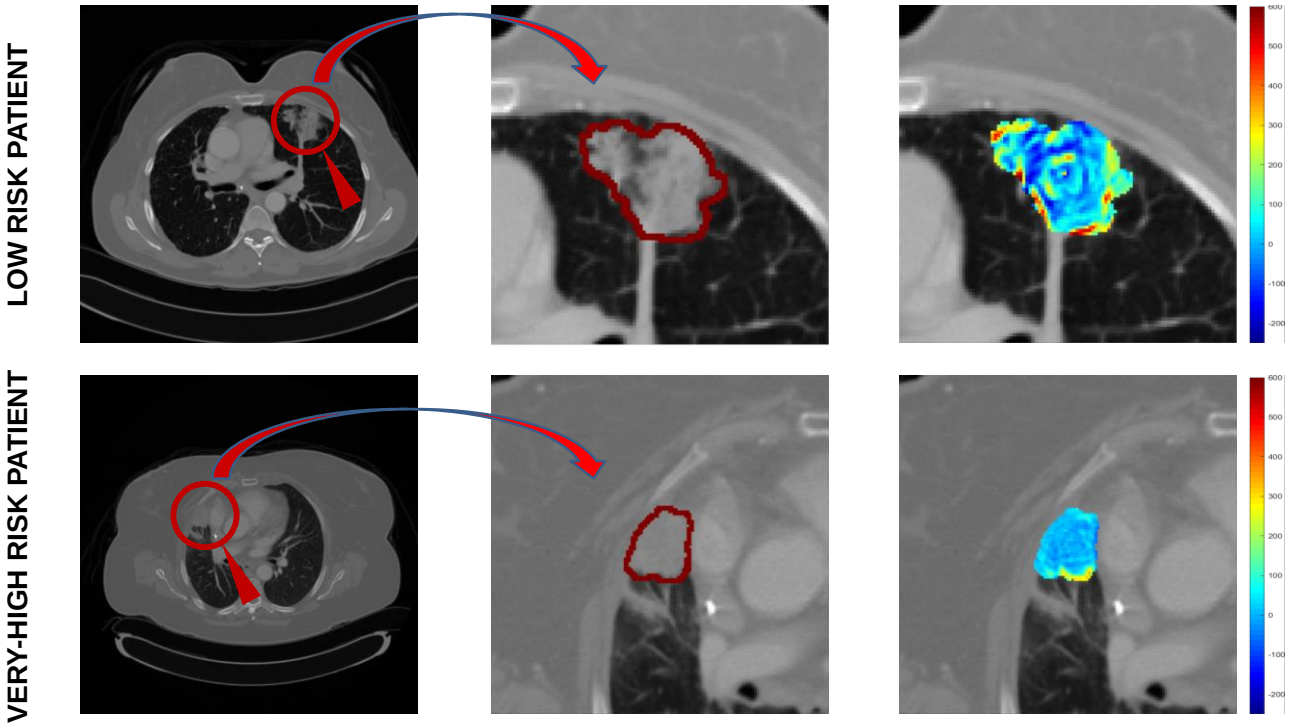


**Supplementary Figure 4**. **Patients on low and very-high risk groups.** First column represents the primary target lesion CT scan. Second column represents the tumor segmentation. Third column represents a gradient image of the segmented area for visualization of the tumor texture. Patient on the top was identified as a low risk patient to immunotherapy and had a less dense tumor phenotype with lower GLCM inverse difference score. Patient on the bottom was identified as a very-high risk patient and had a dense tumor phenotype with higher GLCM inverse score.

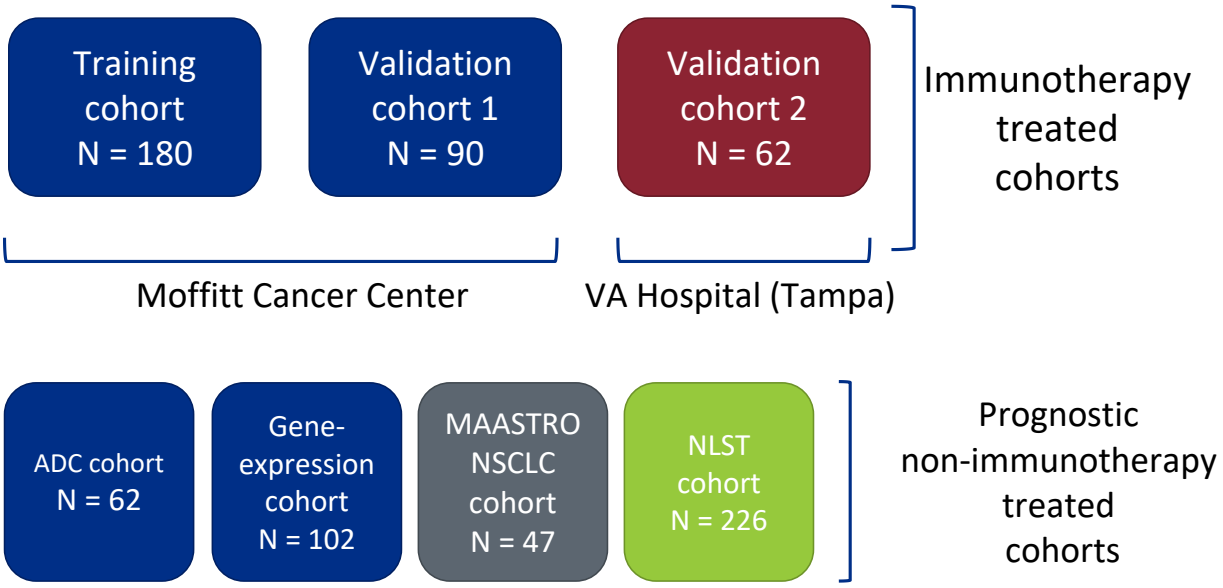


**Supplementary Figure 5. The patient cohorts utilized in this study.** The training cohort was utilized for model building and finding most informative radiomics and clinical covariates. The clinical-radiomics risk-model found in the training cohort were validated in two independent validation cohorts. The prognostic non-immunotherapy cohorts were only used for further validation of the single radiomic feature (GLCM inverse difference) as a pan-signature for survival of lung cancer.

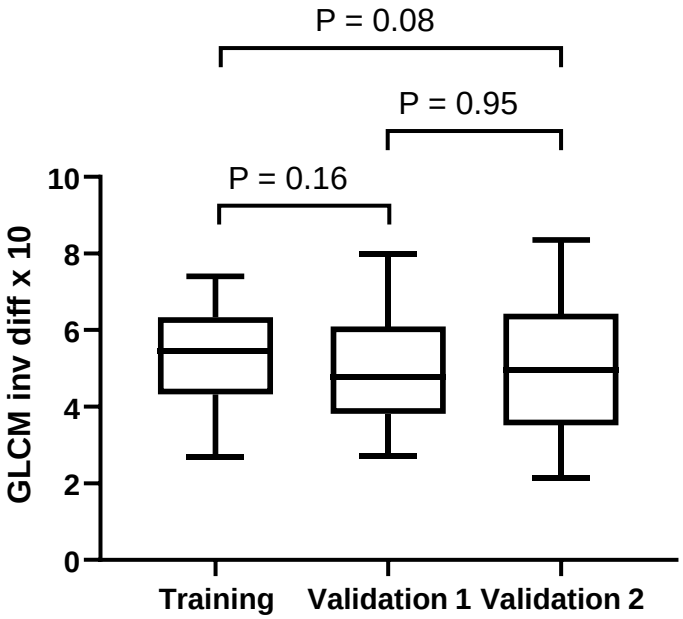


**Supplementary Figure 6**. **Whisker-box plots for GLCM inverse difference.** The mean GLCM inverse difference was not statistically significantly different between all three immunotherapy treated cohorts (Student's *t* test *P* > .05).